creative commons
COMMONS DEED

저작자표시-비영리-변경금지 2.0 대한민국

이용자는 아래의 조건을 따르는 경우에 한하여 자유롭게

- 이 저작물을 복제, 배포, 전송, 전시, 공연 및 방송할 수 있습니다.

다음과 같은 조건을 따라야 합니다:

저작자표시. 귀하는 원저작자를 표시하여야 합니다.

비영리. 귀하는 이 저작물을 영리 목적으로 이용할 수 없습니다.

변경금지. 귀하는 이 저작물을 개작, 변형 또는 가공할 수 없습니다.

- 귀하는, 이 저작물의 재이용이나 배포의 경우, 이 저작물에 적용된 이용허락조건을 명확하게 나타내어야 합니다.
- 저작권자로부터 별도의 허가를 받으면 이러한 조건들은 적용되지 않습니다.

저작권법에 따른 이용자의 권리는 위의 내용에 의하여 영향을 받지 않습니다.

이것은 이용허락규약(Legal Code)을 이해하기 쉽게 요약한 것입니다.

Disclaimer

dCollection

교육학석사 학위논문

Electric Field Cycling-mediated Variations in Defect Distributions Associated with Split-up Behavior of a Ferroelectric Si-doped HfO_2 Thin Film

전기장에 의한 결함분포 변화와 관련된 실리콘이 도핑 된 산화물 하프늄 박막의 Split-up 거동

2020년 8월

서울대학교 대학원

과학교육과 물리전공

송 명 섭

Electric Field Cycling-mediated Variations in Defect Distributions Associated with Split-up Behavior of a Ferroelectric Si-doped HfO_2 Thin Film

전기장에 의한 결함분포 변화와 관련된 실리콘이 도핑 된 산화물 하프늄 박막의 Split-up 거동

지도 교수 채 승 철

이 논문을 교육학석사 학위논문으로 제출함
2020년 8월

서울대학교 대학원
과학교육과 물리전공
송 명 섭

송명섭의 교육학석사 학위논문을 인준함
2020년 8월

위 원 장 _____ 전 동 렬 _____ (인)

부위원장 _____ 조 정 효 _____ (인)

위 원 _____ 채 승 철 _____ (인)

Abstract

We report variations in the characteristic ferroelectric switching time and interface free carrier concentration associated with the wake-up and split-up behaviors of a 4.2 mol % Si-doped HfO_2 thin film. Prior to the development of split-up behavior, the thin films exhibited the wake-up behavior; the remnant polarization increased on repeated external bias cycling. After the wake-up behavior, Si-doped HfO_2 films exhibited degradation of the remnant polarization values and splitting of the ferroelectric switching current peaks when the external bias was swept; this is referred to as split-up behavior. An investigation of the ferroelectric switching dynamics revealed retardation, followed by recovery, of the characteristic switching time for ferroelectric nucleation, coincident with the wake-up and split-up behaviors, respectively. We analyzed the interface free carrier concentration by deriving capacitance-voltage characteristics and revealed that split-up behavior was associated with increased numbers of defects as electric field cycling continued.

Keyword : : Ferroelectricity, HfO_2, Split-up, thin film, defect

Student Number : 2018-27202

Table of Contents

List of table

List of figure

I. Introduction

The ferroelectricity of ultra-thin HfO_2 films has attracted increasing attention given that the films are highly compatible with current complementary metal oxide semiconductor (CMOS) processes [1-4]. The increasing demand for non-volatile universal memory has driven a great deal of research on the maintenance of the ferroelectricity of such films, which have many potential commercial applications. When various dopants were included, HfO_2 films fabricated using the sub-10 nm CMOS process exhibited good ferroelectricity; the remnant polarization P_r was of the order 10 $\mu C/cm^2$ [5, 6]. Such ferroelectric properties of HfO_2 may mitigate the blockage of ferroelectric memory caused by the perovskites [7, 8]. Thus, HfO_2 films exhibiting ferroelectricity may find immediate applications not only in the context of random access memory, but also in the construction of tunneling junctions [9, 10]. However, although non-volatile memory applications using HfO_2 film are maturing, the utility of such ferroelectricity remains debatable; it is unclear whether it is thermally stable and reliable during switching [11, 12].

A detailed understanding of ferroelectricity and the properties thereof in HfO_2 thin films is essential for practical applications. Stabilization of the non-centrosymmetric orthorhombic $Pca2_1$ phase has often been suggested to give rise to ferroelectricity [5, 13, 14]. Prior to commercialization, variations in ferroelectric switching mechanisms, and the characteristics thereof under external bias cycling, must be thoroughly understood. For example, the wake-up [15, 16], fatigue [11, 17-19], and split-up [20] behaviors may be of major concern in terms of the stability of a ferroelectric memory device. Regarding the wake-up behavior, enhancement of spontaneous polarization has been suggested to reflect structural

variations among ferroelectric orthorhombic and non-ferroelectric structural phases (i.e., monoclinic and tetragonal phases). In terms of fatigue behavior, various experimental methods, including first-order reversible curve (FORC) [21] construction, first-principle analysis [22], impedance spectroscopy [19], scanning tunneling electron microscopy [19], and harmonic analysis [17], have attributed the origin of fatigue to variations in bulk defect concentrations [19], modification of interface junction properties [18], or structural decomposition mediated by charge carrier injection [23, 24]. However, the split-up behavior, the splitting of the ferroelectric switching current peaks, has not previously been investigated rigorously, compared with the emergence and enhancement of ferroelectricity in HfO_2 via external field cycling. Thus, a deeper understanding of ferroelectric characteristics in terms of split-up behavior is essential from a practical viewpoint.

A comprehensive study on ferroelectric switching dynamics would clarify the factors governing split-up behavior associated with oxygen vacancies and other defects. Studies on polarization switching over time have aimed to define the types of defects in ferroelectric materials. For example, ferroelectric switching dynamics revealed the presence of dipole defects in polycrystalline $Pb(Zr_xTi_{1-x})O_3$ (poly-PZT) films [25], and the development of distinct interfacial defects when the switching time distributions were asymmetric [26]. Although the split-up behavior of the HfO_2 thin-film ferroelectric switching current has been studied using conventional polarization hysteresis [17] and FORC construction [20], the underlying mechanism requires more attention; a thorough understanding of ferroelectric switching dynamics would reveal the mechanism underlying split-up behavior.

In this Letter, we report the ferroelectric switching dynamics of the split-up behavior of Si-doped HfO_2 thin films. We studied the evolution of ferroelectric properties using the standard polarization-voltage (*P*-*V*) hysteresis approach, and current-voltage (I-V) measurement, during electric field cycling; 8 nm-thick Si-HfO_2 thin films were fabricated via atomic layer deposition (ALD) and capacitance-voltage (C-V) data were obtained to explore the dielectric properties of, and defect distributions in, the interface. The C-V data revealed variations in dielectric properties and the effective interface carrier densities. The split-up behavior when the effective charge density was varied near interfaces was attributable to increased numbers of oxygen vacancies; these controlled the recovery of the characteristic switching time as the ferroelectric switching dynamics evolved.

II. Material and methods

Ferroelectric TiN/Si:HfO_2/TiN capacitors were fabricated on a Si (001) substrate. Prior to fabrication of Si-doped HfO_2 films, the bottom TiN layer was deposited via chemical vapor deposition. The Si-doped HfO_2 film was deposited onto the TiN/Si substrate via ALD. Tetrakis(dimethylamido) hafnium (TDMAH), tetrakis(dimethylamino) silane (4DMAS), and ozone were used for ALD. The top TiN electrode was then deposited via chemical vapor deposition. All specimens were post-annealed at 600°C for 20 s in N_2 to crystallize the Si:HfO_2 films. In terms of electrical and ferroelectric characterization, *P-V* hysteresis and time-dependent dynamic polarization switching [ΔP(t)] were explored using a conventional semiconductor parameter analyzer (model 4200; Keithley) and ferroelectric tester (TF Analyzer 3000; aixACCT Systems).

III. Results and discussion

3.1. Electric field cycling behavior of ferroelectric HfO_2 thin film

Si-doped HfO_2 thin films exhibited initial wake-up and subsequent split-up behaviors. Samples were subjected to 1×10^4 external voltage cycles (3 V at 10 kHz) for wake-up. Next, samples were subjected to 1×10^{10} external voltage cycles (1.6 V at 100 kHz) to allow split-up to be studied [20]. The *P-V* hysteresis measurements were conducted after each wake-up/split-up test. Fig. 1a shows the *P-V* hysteresis loops of Si-doped HfO_2 films (pristine, preset, woken-up, and split-up). The as-grown specimens ("pristine") exhibited pinched hysteresis attributable to the interface pinning effect [17]. As external bias cycling commenced, the remnant polarization increased to 15 $\mu C/cm^2$ and the woken-up specimens developed clear rectangular hysteresis. Such enhancement of the remnant polarization was observed in HfO_2 films containing various dopants; structural phase transitions during cycling enhanced the remnant polarization [15, 19]. As shown in Fig. 1b, after wake-up, ongoing cycling of the external bias induced peak splits in the ferroelectric switching current (split-up behavior). In addition, the remnant polarization of split-up specimens fell as electric field cycling continued (Fig. 1e).

To further investigate in variations of switching current, we conducted first order reversal curves (FORCs) measurement. FORCs measurement shows switching current distribution based on the Preisach model. The bias voltage indicates the asymmetry of preferred direction of polarization by asymmetry of top and bottom

interfacial factors, defect distribution or material difference, etc. Figs. 1c-d show FORCs of ferroelectric Si doped HfO_2 thin film in woken-up and split-up specimen, respectively. The bias voltage merged to near zero voltage that indicates the distribution of switching current homogeneous and the switching peak enhanced in woken-up specimen. After split-up process, two peaks of switching current emerged near at -0.8 and 0.4V that could be contributed to disruption of ferroelectric polarization switching by defect distribution.

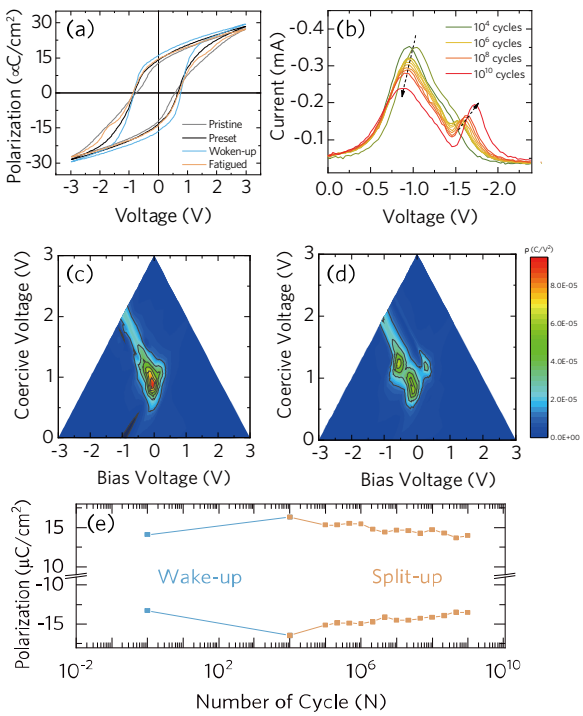

Fig. 1. (a) Polarization-voltage hysteresis of the pristine, preset, woken-up, and split-up cells (Pt/TiN/Si:HfO_2/TiN capacitors). (b) Current-voltage measurements of preset, woken-up, and split-up cells. Experimental switching density acquired from the (c) woken-up and (d) split-up cells. (e) The external field cycle number-dependence of the remnant polarization, which increased and decreased after wake-up and split-up, respectively.

3.2. Investigation of ferroelectric switching dynamics

To characterize the ferroelectricity of pristine, woken-up, and split-up specimens, we studied the ferroelectric switching dynamics under various external voltages. The dynamics of preset, woken-up, and split-up cells were compared in terms of time-dependent changes in the polarization switching [$\Delta P(t)$] values. We investigated switching dynamics after 20 cycles of external bias were applied to pristine specimens; this was associated with a rapid wake-up effect and we refer to these specimens as "preset". We used a bundle of 3-V trapezoidal pulses with a rise time duration of 125 μs; $\Delta P(t)$ values were derived by subtracting the non-ferroelectric from the ferroelectric switching currents (Fig. 2a). A rectangular pulse applied from 140 ns to 1 ms (i.e., a "write" pulse) was used to explore partial switching of ferroelectric polarization (Figs. 2b–d). The switched polarization value ($2P_s$) was measured using a read pulse with a bias opposite to that of the write pulse. After recording $2P_s$, a poling pulse was applied to completely switch the polarization again. To avoid incomplete polarization saturation, the $\Delta P(t)/2P_s$ curves were obtained using a voltage higher than that of the coercive field. The detailed measurement method has been described earlier [16]. Preset, woken-up, and split-up specimens exhibited typical polarization switching behaviors; polarization increased as the amplitude and application time of the external voltage increased (Figs. 2b–d). All specimens exhibited increased $\Delta P(t)/2Ps$ ratios as the external bias increased from 2.0 to 3.0 V.

Experimentally, ferroelectric switching is characterized by an inhomogeneous distribution of local nucleation times, followed by polarization reversal mediated

by limited nucleation switching [16, 27-29]. Ferroelectric switching is governed by both nucleation and subsequent domain growth [30]. Polarization switching kinetics have been modeled using (1) the Kolmogorov-Avrami-Ishibashi (KAI) [31, 32] method and (2) a nucleation-limited-switching (NLS) approach [33]. The KAI model assumes that both homogeneous nucleation and unrestricted domain growth are statistical in nature [31, 32]. The NLS model assumes that polarization switching is limited by domain nucleation, and considers that a polycrystalline film is an ensemble of microscopic regions that are independent in terms of their switching kinetics [33]. For polycrystalline ferroelectric HfO_2 thin films, experiments have suggested that polarization switching is best modeled using the NLS approach [8, 29, 34]. Therefore, we fitted the $\Delta P(t)/2P_s$ values using an NLS model featuring a Lorentzian distribution of the characteristic switching time, as shown in Equations (1) and (2) [25]:

$$\frac{\Delta P(t)}{2P_s} = \int_{-\infty}^{\infty}\left[1 - exp\left\{-\left(\frac{t}{t_0}\right)^n\right\}\right] F(log\, t_0)\, d(log\, t_0) \tag{1}$$

with:

$$F(log\, t_0) = \frac{A}{\pi}\left[\frac{w}{(log\, t_0 - log\, t_1)^2 + w^2}\right] \tag{2}$$

where A, w, and $logt_1$ are a normalization constant, the half-width at half-maximum of the distribution, and the mean distribution value, respectively. The solid lines in Figs. 2b–d indicate that polarization switching was well-described by the NLS model when there was a Lorentzian distribution.

The switching time of ferroelectric nucleation was retarded, but then recovered, in woken-up and split-up specimens, respectively. Fig. 3a shows the deconvoluted Lorentzian distribution used when constructing the fit lines of the solid ferroelectric switching dynamics curves of Figs. 2b–d. The peak positions in Fig. 3a are the characteristic switching times ($\log t_0$ values) of the preset, woken-up, and split-up specimens. For woken-up specimens, the characteristic switching times of the peak positions were retarded, and the peaks were sharpened (blue dashed-dotted lines in Fig. 3a). For split-up specimens, the retarded times recovered and the distributions became broader again (yellow dashed lines in Fig. 3a). Fig. 3b shows the characteristic ferroelectric switching times extracted from Fig. 3a. Distribution sharpening and broadening, as well as switching time retardation and recovery, can be explained by the changes in defect concentrations associated with ferroelectric polarization switching.

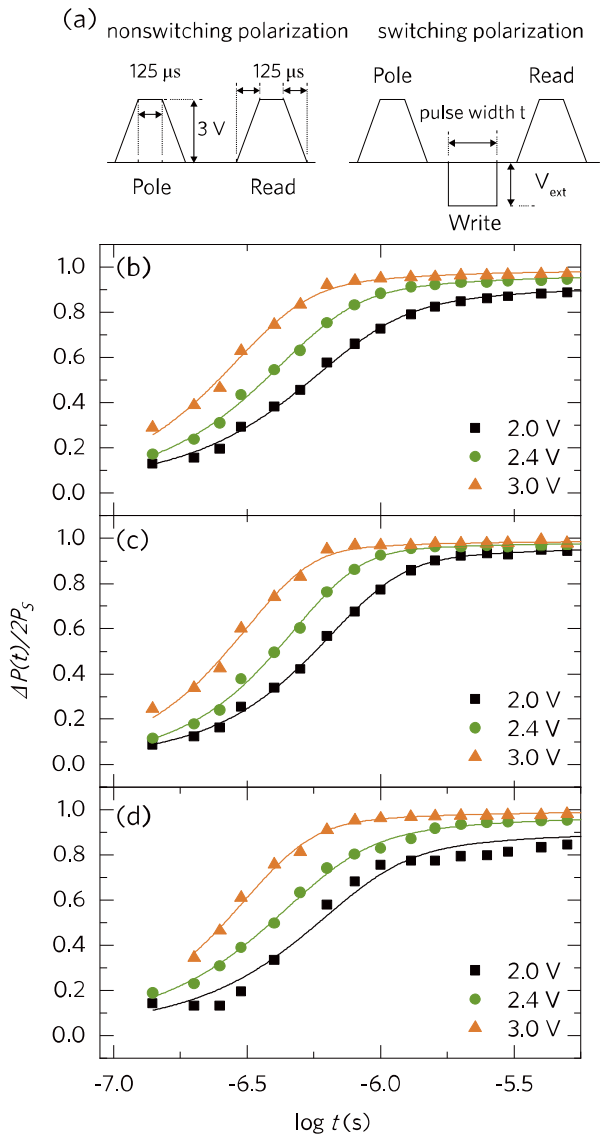

Fig. 2. (a) Schematic of the pulse trains used to measure non-switching and switching polarization. Time-dependent switched polarization [$\Delta P(t)$] as a function of the external voltage (V_{ext}) from 2.0 to 3.0 V at room temperature for (b) preset, (c) woken-up, and (d) split-up cells. The solid lines correspond to the fitting results obtained using the nucleation-limited switching (NLS) model with a Lorentzian distribution of the characteristic switching time.

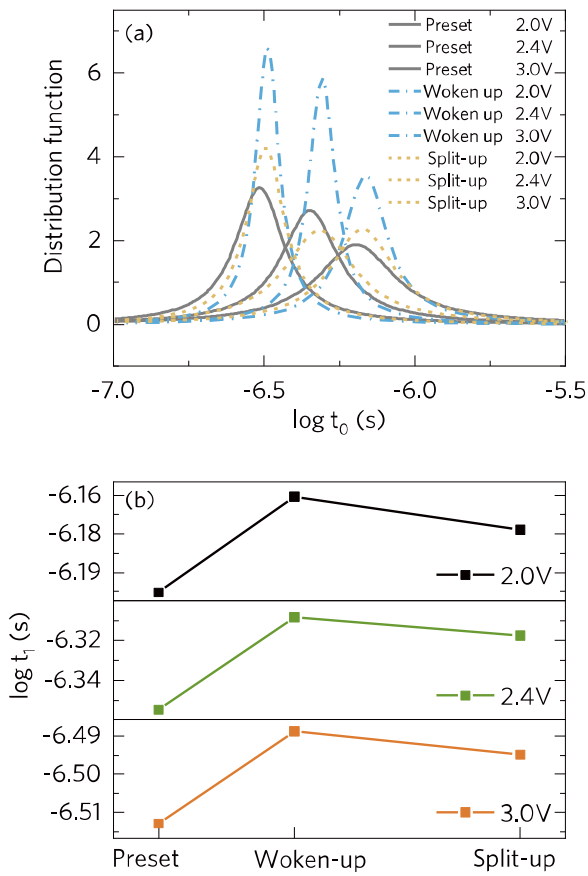

Fig. 3. (a) Lorentzian distributions of the fitting functions for the time-dependent switched polarization shown in Figs. 2b–d of the preset, woken-up, and split-up cells. (b) The extracted characteristic switching time values of the preset, woken-up, and split-up cells when the external voltage varied.

Inhomogeneous switching and changes in polarization switching time are attributable to changes in defect density; this affects local field distribution, where defects serve as pinning sites for domain wall motion inside films [18, 23-25]. For example, a dipole defect aligned antiparallel to the local lattice polarization impedes both nucleation and domain growth. However, a parallel defect dipole enhances both nucleation and domain growth [35]. Also, charge defects, oxygen vacancies, depletion layers, non-ferroelectric structural phases, and pinned domain orientations all trigger inhomogeneous switching behavior [15, 18, 36]. Such defects, and the associated charge-trapping, influence the field distribution over all film layers [37]. The ferroelectric layer encounters a reduced electric field, which either impedes domain propagation [38] or reduces the number of switching domains if the electric field is less than the coercive field [18]. Local defect-related variations in field distribution reduce the nucleation time and average domain size [39, 40]. Film disorders caused by defects serve as nucleation seeds and the amount of activation energy required for domain nucleation decreases [40]. For woken-up specimens, reduced defect density decreases disorder, in turn triggering a more homogeneous switching distribution, followed by retardation of the polarization switching time and marked redistribution of the characteristic ferroelectric switching time. These effects combine to render the inhomogeneity of the switching distribution, and to retard (and then allow recovery of) the characteristic switching time during wake-up and split-up, respectively.

3.3. Changes of interfacial property

During electric field cycling, defect distributions change especially at film interfaces. A defect-rich interfacial layer is formed during deposition of the HfO_2 onto bottom and top TiN electrodes [41, 42]. Repeat electric field cycling induces redistribution of initial oxygen vacancies [43]. It is well-known that repeat cycling generates defects, including oxygen vacancies [44]. It has been suggested that oxygen vacancies are created in, and then migrate from, film interfaces during electric field cycling [45, 46].

To explore variations in interface structure, we performed C-V measurements on preset, woken-up, and spilt-up specimens of Si-HfO_2 films. The free carrier concentration derived from the $1/C^2$-V plots has been investigated at the interface of the metal-semiconductor junctions. The metal-ferroelectric-metal junction has been considered as two back-to-back metal-semiconductor junctions [47, 48] where $1/C^2$-V plots also revealed the many metal-ferroelectric junction properties similar to the metal-semiconductor junction [49-54]. Accordingly, the split-up behavior with respect to the junction properties can be understood by utilizing the capacitance measurement.

Variations in free carrier concentration levels may be calculated via analysis of the interface depletion capacitance [47, 55, 56]. The depletion capacitance (C_d) attributable to a small AC signal is defined as [57]:

$$C_d = \frac{\varepsilon_r \varepsilon_0 A}{W} = \frac{\varepsilon_r \varepsilon_0 A}{\sqrt{\frac{2\varepsilon_r \varepsilon_0}{qN_a}(V_{bi} - V)}} \tag{3}$$

where ε_r, ε_0, A, N_a, V_{bi}, V, and q are the dielectric constant of the film, permittivity of free space, electrode area, free carrier concentration, built-in potential, applied bias, and charge, respectively. When Equation (3) is used to analyze the $1/C^2$-V curves, the free carrier concentration (N_a values) can be determined.

Fig. 4a shows the C-V hysteresis curves for preset, woken-up, and split-up specimens, respectively. The clear hysteresis evident in Fig. 4a reflects the ferroelectricity of the preset, woken-up, and split-up specimens. The peaks in C-V curves are associated with polarization reversal and indicate the transition of the depletion capacitance from the bottom to top and top to bottom Schottky contacts. The peaks are in fact same with the coercive voltage of polarization switching which is represented in Fig. 1. But the coercive voltage in C-V measurement is smaller than coercive voltage in P-V or I-V hysteresis because the C-V curve is a quasi-static measurement. Fig. 4b shows the free carrier concentration-voltage behaviors calculated from Equation (3) when sweep down from 2 V to – 2 V for preset, woken-up, and split-up specimens, respectively. In Fig. 4b, the sign of calculated N_a values changes abruptly near 0.5 V which correspond with the coercive voltage in C-V measurement. This is not due to the change in the carrier type but the aforementioned transition of the depletion capacitance which result in sign change in the $d(1/C^2)/dV$ derivation. Except the region where the polarization switching occurs, the free carrier concentration was well estimated without the influence of the polarization reversal on the measured capacitance. Note that the linearity of $1/C^2$-V plots and the constant N_a values indicate that the effect of ferroelectric polarization switching is negligible (inset in Fig. 4b). In the saturated region, the N_a value of woken up specimen is 2.79×10^{18} cm^{-3} which is lower than

the preset specimen 3.29 × 10^{18} cm^{-3}. After the split-up process, the N_a value rebounded 2.92 × 10^{18} cm^{-3} (Table 1). Although the N_a values differed between sweep-up and sweep-down because of interface asymmetry, the trends associated with continued electric field cycling were identical.

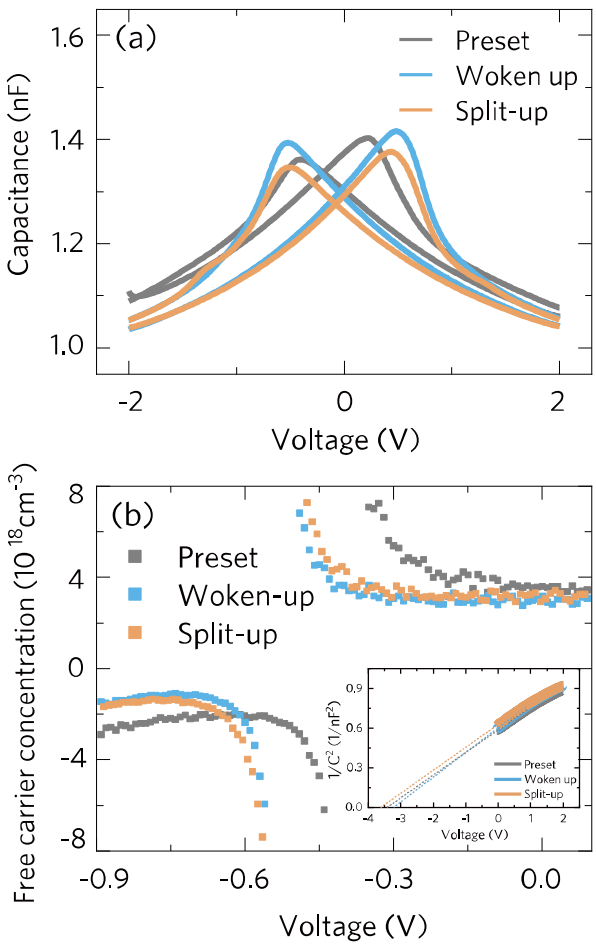

Fig. 4. (a) Capacitance-voltage characteristics and (b) free carrier concentration-voltage behavior of Si:HfO_2 thin film for the preset, woken-up, and split-up cells. Inset shows linear fitting of $1/C^2$-V plots for preset, woken-up, and split-up cells in region where ferroelectric switching is negligible.

Table 1. Free carrier concentrations of Si:HfO_2 thin film capacitors according to the extent of electric field cycling

	Free carrier concentration (cm^{-3})	
	Sweep up	Sweep down
Preset	3.29E+18	3.34E+18
Woken-up	2.79E+18	3.06E+18
Split-up	2.92E+18	3.29E+18

Variations in local electric fields that interfere with ferroelectric polarization switching are attributable to changes in the density of oxygen vacancies. Such vacancies near interfaces trap charges that interfere with free polarization switching [58]. A change in the number of oxygen vacancies can be estimated by measuring the free carrier concentration. We used Equation (3) to derive changes in the free carrier concentration of woken-up and split-up specimens, which indicate changes in the number of oxygen vacancies at the film interface [47]. Redistribution of such vacancies decreased free carrier concentration from 3.29×10^{18} to 2.79×10^{18} cm^{-3} during wake-up. However, after split-up process, the concentration increased from 2.79×10^{18} to 2.92×10^{18} cm^{-3}. Thus, further electric field cycling generated oxygen vacancies near the interface, accompanied by split-up behavior. Such changes in the number of oxygen vacancies with continued field cycling causes both the initial retardation, and subsequent recovery, of the characteristic switching time.

IV. Conclusions

In summary, we investigated the polarization switching dynamics of, and obtained C-V data on, woken-up and split-up Si-doped HfO_2 thin films. The peak splits of ferroelectric switching currents were evident in the split-up specimens; the remnant polarization decreased on repeat electric field cycling. The polarization switching of polycrystalline ferroelectric Si-doped HfO_2 was well-described by the NLS model with a Lorentzian distribution of the characteristic switching time for nucleation. In split-up specimens, the lag in the characteristic switching time (attributable to defect redistribution during wake-up) was gradually eliminated, and the shape of the distribution broadened. We used C-V data to estimate defect densities near the interface. Given the observed ferroelectric switching dynamics and derived C-V measurements, we found that split-up behavior was attributable to changes in oxygen vacancy density; such changes induced local fields that interfered with ferroelectric polarization switching.

References

[1] J. Müller, T.S. Böscke, S. Müller, E. Yurchuk, P. Polakowski, J. Paul, D. Martin, T. Schenk, K. Khullar, A. Kersch, W. Weinreich, S. Riedel, K. Seidel, A. Kumar, T.M. Arruda, S.V. Kalinin, T. Schlösser, R. Boschke, R.v. Bentum, U. Schröder, T. Mikolajick, Ferroelectric hafnium oxide: A CMOS -compatible and highly scalable approach to future ferroelectric memories, in: Int. Electron Devices Meet., 2013, 10.18.11-10.18.14. http://doi.org/10.1109/IEDM.2013.6724605.

[2] C. Cheng, A. Chin, Low-Leakage-Current DRAM-Like Memory Using a One-Transistor Ferroelectric MOSFET With a Hf-Based Gate Dielectric, IEEE Electron. Device Lett. 35 (2014) 138-140. http://doi.org/10.1109/LED.2013.2290117.

[3] S. Mueller, J. Müller, R. Hoffmann, E. Yurchuk, T. Schlösser, R. Boschke, J. Paul, M. Goldbach, T. Herrmann, A. Zaka, U. Schröder, T. Mikolajick, From MFM Capacitors Toward Ferroelectric Transistors: Endurance and Disturb Characteristics of HfO_2-Based FeFET Devices, IEEE Trans. Device Mater. 60 (2013) 4199-4205. http://doi.org/10.1109/TED.2013.2283465.

[4] E. Yurchuk, J. Müller, J. Paul, T. Schlösser, D. Martin, R. Hoffmann, S. Müeller, S. Slesazeck, U. Schröeder, R. Boschke, R.v. Bentum, T. Mikolajick, Impact of Scaling on the Performance of HfO_2-Based Ferroelectric Field Effect Transistors, IEEE Trans. Device Mater. 61 (2014) 3699-3706. http://doi.org/10.1109/TED.2014.2354833.

[5] T.S. Böscke, J. Müller, D. Bräuhaus, U. Schröder, U. Böttger, Ferroelectricity in hafnium oxide thin films, Appl. Phys. Lett. 99 (2011) 102903. http://doi.org/10.1063/1.3634052.

[6] M.H. Park, Y.H. Lee, H.J. Kim, Y.J. Kim, T. Moon, K.D. Kim, J. Müller, A. Kersch, U. Schroeder, T. Mikolajick, C.S. Hwang, Ferroelectricity and Antiferroelectricity of Doped Thin HfO_2-Based Films, Adv. Mater. 27 (2015) 1811-1831. http://doi.org/10.1002/adma.201404531.

[7] J. Müller, T.S. Böscke, U. Schröder, S. Mueller, D. Bräuhaus, U. Böttger, L. Frey, T. Mikolajick, Ferroelectricity in Simple Binary ZrO_2 and HfO_2, Nano Lett. 12 (2012) 4318-4323. http://doi.org/10.1021/nl302049k.

[8] U. Schroeder, S. Mueller, J. Mueller, E. Yurchuk, D. Martin, C. Adelmann, T. Schloesser, R. van Bentum, T. Mikolajick, Hafnium Oxide Based CMOS Compatible Ferroelectric Materials, ECS Journal of Solid State Science and Technology 2 (2013) N69-N72. http://doi.org/10.1149/2.010304jss.

[9] F. Ambriz-Vargas, G. Kolhatkar, M. Broyer, A. Hadj-Youssef, R. Nouar, A. Sarkissian, R. Thomas, C. Gomez-Yáñez, M.A. Gauthier, A. Ruediger, A Complementary Metal Oxide Semiconductor Process-Compatible Ferroelectric Tunnel Junction, ACS Appl. Mater. Interfaces 9 (2017) 13262-13268. http://doi.org/10.1021/acsami.6b16173.

[10] F. Ambriz-Vargas, G. Kolhatkar, R. Thomas, R. Nouar, A. Sarkissian, C. Gomez-Yáñez, M.A. Gauthier, A. Ruediger, Tunneling electroresistance effect in a $Pt/Hf_{0.5}Zr_{0.5}O_2/Pt$ structure, Appl. Phys. Lett. 110 (2017) 093106. http://doi.org/10.1063/1.4977028.

[11] E. Yurchuk, S. Mueller, D. Martin, S. Slesazeck, U. Schroeder, T. Mikolajick, J. Müller, J. Paul, R. Hoffmann, J. Sundqvist, T. Schlösser, R. Bosc

hke, R.v. Bentum, M. Trentzsch, Origin of the endurance degradation in the novel HfO_2-based 1T ferroelectric non-volatile memories, in: 2014 IEEE International Reliability Physics Symposium, 2014, 2E.5.1-2E.5.5. http://doi.org/10.1109/IRPS.2014.6860603.

[12] D. Zhou, Y. Guan, M.M. Vopson, J. Xu, H. Liang, F. Cao, X. Dong, J. Mueller, T. Schenk, U. Schroeder, Electric field and temperature scaling of polarization reversal in silicon doped hafnium oxide ferroelectric thin films, Acta Mater 99 (2015) 240-246. http://doi.org/https://doi.org/10.1016/j.actamat.2015.07.035.

[13] X. Sang, E.D. Grimley, T. Schenk, U. Schroeder, J.M. LeBeau, On the structural origins of ferroelectricity in HfO_2 thin films, Appl. Phys. Lett. 106 (2015) 162905. http://doi.org/10.1063/1.4919135.

[14] R. Materlik, C. Künneth, A. Kersch, The origin of ferroelectricity in $Hf_{1-x}Zr_xO_2$: A computational investigation and a surface energy model, J. Appl. Phys. 117 (2015) 134109. http://doi.org/10.1063/1.4916707.

[15] D. Zhou, J. Xu, Q. Li, Y. Guan, F. Cao, X. Dong, J. Müller, T. Schenk, U. Schröder, Wake-up effects in Si-doped hafnium oxide ferroelectric thin films, Appl. Phys. Lett. 103 (2013) 192904. http://doi.org/10.1063/1.4829064.

[16] T.Y. Lee, K. Lee, H.H. Lim, M.S. Song, S.M. Yang, H.K. Yoo, D.I. Suh, Z. Zhu, A. Yoon, M.R. MacDonald, X. Lei, H.Y. Jeong, D. Lee, K. Park, J. Park, S.C. Chae, Ferroelectric Polarization-Switching Dynamics and Wake-Up Effect in Si-Doped HfO_2, ACS Appl. Mater. Interfaces 11 (2019) 3142-3149. http://doi.org/10.1021/acsami.8b11681.

[17] T. Schenk, U. Schroeder, M. Pešić, M. Popovici, Y.V. Pershin, T. Mik

olajick, Electric Field Cycling Behavior of Ferroelectric Hafnium Oxide, ACS Appl. Mater. Interfaces 6 (2014) 19744-19751. http://doi.org/10.1021/am504837r.

[18] M. Pešić, F.P.G. Fengler, L. Larcher, A. Padovani, T. Schenk, E.D. Grimley, X. Sang, J.M. LeBeau, S. Slesazeck, U. Schroeder, T. Mikolajick, Physical Mechanisms behind the Field-Cycling Behavior of HfO2-Based Ferroelectric Capacitors, Advanced Functional Materials 26 (2016) 4601-4612. http://doi.org/10.1002/adfm.201600590.

[19] E.D. Grimley, T. Schenk, X. Sang, M. Pešić, U. Schroeder, T. Mikolajick, J.M. LeBeau, Structural Changes Underlying Field-Cycling Phenomena in Ferroelectric HfO_2 Thin Films, Adv. Electron. Mater. 2 (2016) 1600173. http://doi.org/10.1002/aelm.201600173.

[20] T. Schenk, M. Hoffmann, J. Ocker, M. Pešić, T. Mikolajick, U. Schroeder, Complex Internal Bias Fields in Ferroelectric Hafnium Oxide, ACS Appl. Mater. Interfaces 7 (2015) 20224-20233. http://doi.org/10.1021/acsami.5b05773.

[21] C. Wang, X. Yang, Z. Wang, C. He, X. Long, Investigation of switching behavior of acceptor-doped ferroelectric ceramics, Acta Mater 170 (2019) 100-108. http://doi.org/https://doi.org/10.1016/j.actamat.2019.03.033.

[22] Y. Zhou, Y.K. Zhang, Q. Yang, J. Jiang, P. Fan, M. Liao, Y.C. Zhou, The effects of oxygen vacancies on ferroelectric phase transition of HfO_2-based thin film from first-principle, Comput. Mater. Sci. 167 (2019) 143-150. http://doi.org/https://doi.org/10.1016/j.commatsci.2019.05.041.

[23] F. Huang, X. Chen, X. Liang, J. Qin, Y. Zhang, T. Huang, Z. Wang, B. Peng, P. Zhou, H. Lu, L. Zhang, L. Deng, M. Liu, Q. Liu, H. Tian, L.

Bi, Fatigue mechanism of yttrium-doped hafnium oxide ferroelectric thin film s fabricated by pulsed laser deposition, Phys. Chem. Chem. Phys. 19 (2017) 3486-3497. http://doi.org/10.1039/C6CP07501K.

[24] X. Liu, D. Zhou, Y. Guan, S. Li, F. Cao, X. Dong, Endurance properti es of silicon-doped hafnium oxide ferroelectric and antiferroelectric-like thin films: A comparative study and prediction, Acta Mater 154 (2018) 190-198. http://doi.org/https://doi.org/10.1016/j.actamat.2018.05.033.

[25] J.Y. Jo, H.S. Han, J.G. Yoon, T.K. Song, S.H. Kim, T.W. Noh, Domai n Switching Kinetics in Disordered Ferroelectric Thin Films, Phys. Rev. Lett. 99 (2007) 267602. http://doi.org/10.1103/PhysRevLett.99.267602.

[26] T.H. Kim, S.H. Baek, S.M. Yang, Y.S. Kim, B.C. Jeon, D. Lee, J.-S. Chung, C.B. Eom, J.-G. Yoon, T.W. Noh, Polarity-dependent kinetics of ferr oelectric switching in epitaxial $BiFeO_3$(111) capacitors, Appl. Phys. Lett. 99 (2011) 012905. http://doi.org/10.1063/1.3609235.

[27] H. Mulaosmanovic, J. Ocker, S. Müller, U. Schroeder, J. Müller, P. Pol akowski, S. Flachowsky, R. van Bentum, T. Mikolajick, S. Slesazeck, Switc hing Kinetics in Nanoscale Hafnium Oxide Based Ferroelectric Field-Effect Transistors, ACS Appl. Mater. Interfaces 9 (2017) 3792-3798. http://doi.org/1 0.1021/acsami.6b13866.

[28] P. Buragohain, C. Richter, T. Schenk, H. Lu, T. Mikolajick, U. Schroe der, A. Gruverman, Nanoscopic studies of domain structure dynamics in ferr oelectric La:HfO_2 capacitors, Appl. Phys. Lett. 112 (2018) 222901. http://doi. org/10.1063/1.5030562.

[29] N. Gong, X. Sun, H. Jiang, K.S. Chang-Liao, Q. Xia, T.P. Ma, Nuclea tion limited switching (NLS) model for HfO_2-based metal-ferroelectric-metal

(MFM) capacitors: Switching kinetics and retention characteristics, Appl. Phys. Lett. 112 (2018) 262903. http://doi.org/10.1063/1.5010207.

[30] M. Dawber, K.M. Rabe, J.F. Scott, Physics of thin-film ferroelectric oxides, Rev. Mod. Phys 77 (2005) 1083-1130. http://doi.org/10.1103/RevModPhys.77.1083.

[31] M. Avrami, Kinetics of Phase Change. II Transformation-Time Relations for Random Distribution of Nuclei, The Journal of Chemical Physics 8 (1940) 212-224. http://doi.org/10.1063/1.1750631.

[32] Y. Ishibashi, Y. Takagi, Note on Ferroelectric Domain Switching, Jpn. J. Appl. Phys 31 (1971) 506-510. http://doi.org/10.1143/JPSJ.31.506.

[33] A.K. Tagantsev, I. Stolichnov, N. Setter, J.S. Cross, M. Tsukada, Non-Kolmogorov-Avrami switching kinetics in ferroelectric thin films, Phys. Rev. B 66 (2002) 214109. http://doi.org/10.1103/PhysRevB.66.214109.

[34] S. Mueller, S.R. Summerfelt, J. Muller, U. Schroeder, T. Mikolajick, Ten-Nanometer Ferroelectric Si:HfO_2 Films for Next-Generation FRAM Capacitors, IEEE Electron. Device Lett. 33 (2012) 1300-1302. http://doi.org/10.1109/LED.2012.2204856.

[35] P. Erhart, P. Träskelin, K. Albe, Formation and switching of defect dipoles in acceptor-doped lead titanate: A kinetic model based on first-principles calculations, Phys. Rev. B 88 (2013) 024107. http://doi.org/10.1103/PhysRevB.88.024107.

[36] S.D. Hyun, H.W. Park, Y.J. Kim, M.H. Park, Y.H. Lee, H.J. Kim, Y.J. Kwon, T. Moon, K.D. Kim, Y.B. Lee, B.S. Kim, C.S. Hwang, Dispersion in Ferroelectric Switching Performance of Polycrystalline $Hf_{0.5}Zr_{0.5}O_2$ Thin Films, ACS Appl. Mater. Interfaces 10 (2018) 35374-35384. http://doi.org/10.10

21/acsami.8b13173.

[37] M. Pesic, F.P.G. Fengler, S. Slesazeck, U. Schroeder, T. Mikolajick, L. Larcher, A. Padovani, Root cause of degradation in novel HfO_2-based ferro electric memories, in: 2016 IEEE International Reliability Physics Symposiu m (IRPS), 2016, MY-3-1-MY-3-5. http://doi.org/10.1109/IRPS.2016.7574619.

[38] S.M. Yang, J.-G. Yoon, T.W. Noh, Nanoscale studies of defect-mediate d polarization switching dynamics in ferroelectric thin film capacitors, Curr. Appl. Phys. 11 (2011) 1111-1125. http://doi.org/https://doi.org/10.1016/j.cap.20 11.05.017.

[39] A. Pramanick, A.D. Prewitt, J.S. Forrester, J.L. Jones, Domains, Domai n Walls and Defects in Perovskite Ferroelectric Oxides: A Review of Presen t Understanding and Recent Contributions, Crit. Rev. Solid State Mater. Sci. 37 (2012) 243-275. http://doi.org/10.1080/10408436.2012.686891.

[40] A.N. Morozovska, S.V. Svechnikov, E.A. Eliseev, B.J. Rodriguez, S. Je sse, S.V. Kalinin, Local polarization switching in the presence of surface-cha rged defects: Microscopic mechanisms and piezoresponse force spectroscopy observations, Phys. Rev. B 78 (2008) 054101. http://doi.org/10.1103/PhysRev B.78.054101.

[41] M. Pešić, S. Knebel, K. Cho, C. Jung, J. Chang, H. Lim, N. Kolomiiet s, V.V. Afanas'ev, T. Mikolajick, U. Schroeder, Conduction barrier offset en gineering for DRAM capacitor scaling, Solid State Electron. 115 (2016) 133-139. http://doi.org/https://doi.org/10.1016/j.sse.2015.08.012.

[42] W. Weinreich, A. Shariq, K. Seidel, J. Sundqvist, A. Paskaleva, M. Le mberger, A.J. Bauer, Detailed leakage current analysis of metal–insulator–met al capacitors with ZrO_2, $ZrO_2/SiO_2/ZrO_2$, and $ZrO_2/Al_2O_3/ZrO_2$ as dielectric a

nd TiN electrodes, J. Vac. Sci. Technol. B 31 (2013) 01A109. http://doi.org/10.1116/1.4768791.

[43] S. Starschich, S. Menzel, U. Böttger, Evidence for oxygen vacancies movement during wake-up in ferroelectric hafnium oxide, Appl. Phys. Lett. 108 (2016) 032903. http://doi.org/10.1063/1.4940370.

[44] E. Cartier, A. Kerber, Stress-induced leakage current and defect generation in nFETs with HfO_2/TiN gate stacks during positive-bias temperature stress, in: 2009 IEEE International Reliability Physics Symposium, 2009, 486-492. http://doi.org/10.1109/IRPS.2009.5173301.

[45] J.F. Scott, M. Dawber, Oxygen-vacancy ordering as a fatigue mechanism in perovskite ferroelectrics, Appl. Phys. Lett. 76 (2000) 3801-3803. http://doi.org/10.1063/1.126786.

[46] C. Brennan, Model of ferroelectric fatigue due to defect/domain interactions, Ferroelectrics 150 (1993) 199-208. http://doi.org/10.1080/00150199308008705.

[47] L. Pintilie, M. Alexe, Metal-ferroelectric-metal heterostructures with Schottky contacts. I. Influence of the ferroelectric properties, J. Appl. Phys. 98 (2005) 124103. http://doi.org/10.1063/1.2148622.

[48] L. Pintilie, I. Boerasu, M. Gomes, T. Zhao, R. Ramesh, M. Alexe, Metal-ferroelectric-metal structures with Schottky contacts. II. Analysis of the experimental current-voltage and capacitance-voltage characteristics of Pb(Zr, Ti)O_3 thin films, J. Appl. Phys. 98 (2005) 124104. http://doi.org/https://doi.org/10.1063/1.2148623.

[49] P. Zubko, D. Jung, J. Scott, Electrical characterization of $PbZr_{0.4}Ti_{0.6}O_3$ capacitors, J. Appl. Phys. 100 (2006) 114113. http://doi.org/10.1063/1.238247

9.

[50] S. Kotru, V. Batra, V. Harshan, Electrical behavior of $Pb_{0.95}La_{0.05}Zr_{0.54}Ti_{0.46}O_3$ thin film based capacitors: Influence of space charge region, J. Appl. Phys. 124 (2018) 034101. http://doi.org/10.1063/1.5031457.

[51] W. Zhang, Y. Gao, L. Kang, M. Yuan, Q. Yang, H. Cheng, W. Pan, J. Ouyang, Space-charge dominated epitaxial $BaTiO_3$ heterostructures, Acta Mater 85 (2015) 207-215. https://doi.org/10.1016/j.actamat.2014.10.063.

[52] L. Pintilie, M. Lisca, M. Alexe, Polarization reversal and capacitance-voltage characteristic of epitaxial $Pb(Zr, Ti)O_3$ layers, Appl. Phys. Lett. 86 (2005) 192902. http://doi.org/10.1063/1.1926403.

[53] L. Pintilie, V. Stancu, L. Trupina, I. Pintilie, Ferroelectric schottky diode behavior from a $SrRuO_3$-$Pb(Zr_{0.2}Ti_{0.8})O_3$-Ta structure, Phys. Rev. B 82 (2010) 085319. https://doi.org/10.1103/PhysRevB.82.085319.

[54] N. Tayebi, S. Kim, R.J. Chen, Q. Tran, N. Franklin, Y. Nishi, Q. Ma, V. Rao, Tuning the built-in electric field in ferroelectric $Pb(Zr_{0.2}Ti_{0.8})O_3$ films for long-term stability of single-digit nanometer inverted domains, Nano Lett. 12 (2012) 5455-5463. https://doi.org/10.1021/nl302911k.

[55] D.K. Schroder, Semiconductor material and device characterization, John Wiley & Sons, New Jersey, 2015.

[56] S. Kotru, V. Batra, V.N. Harshan, Electrical behavior of $Pb_{0.95}La_{0.05}Zr_{0.54}Ti_{0.46}O_3$ thin film based capacitors: Influence of space charge region, J. Appl. Phys. 124 (2018) 034101. http://doi.org/10.1063/1.5031457.

[57] S.M. Sze, K.K. Ng, Physics of Semiconductor Devices, Wiley, New Jersey, 2006.

[58] J.L. Gavartin, D.M. Ramo, A.L. Shluger, G. Bersuker, B.H. Lee, Negati

ve oxygen vacancies in HfO_2 as charge traps in high-k stacks, Appl. Phys. Lett. 89 (2006) 082908. http://doi.org/10.1063/1.2236466.

Appendix

<A.1> Experimental method for first order reversal curves (FORCs) measurement

A.1.1. Derivation of FORC measurement

The first order reversal curves (FORCs) measurement shows the switching density (Preisach density) on the switching field distribution.

The simplest way to calculate this switching density is as follows: To derivate the switching density, the polarization switching current have to be obtained by field sweeps starting at saturated field increasing the amplitude of reversal field as shown in Fig A1. The switching density is defined as the mixed second derivative of the polarization with respect to the reversal field E_r and actual field E, i.e., field region from the reversal field to saturated field:

$$\rho(E_r, E) = \frac{1}{2} \cdot \frac{\partial^2 P_{FORC}(E_r, E)}{\partial E_r \partial E} = \frac{1}{2 \cdot \dot{E}} \frac{\partial j_{FORC}(E_r, E)}{\partial E_r} \approx \frac{1}{2\dot{E}} \frac{j_{FORC}(E_{r,i}, E) - j_{FORC}(E_{r,i-1}, E)}{E_{r,i} - E_{r,i-1}} \quad \text{(A1)}$$

For each i-th reversal field $E_{r,i}$ plotted as the y-axis, the difference in the measured switching current response to the current for the previous reversal field is plotted versus the actual field E. It is recommended to adjust the measuring sample points as amplitude of reversal field in instrument system or fitting the switching current to aligning actual field E_i. In this paper we represented the FORC distribution versus the coordinates of coercive voltage V_c and the bias voltage V_{bias} representing respectively coercive field E_c and the bias field E_{bias} by using coordinate transformation:

$$V_c = \frac{V - V_r}{2}, V_{bias} = \frac{V + V_r}{2} \quad \text{(A2)}$$

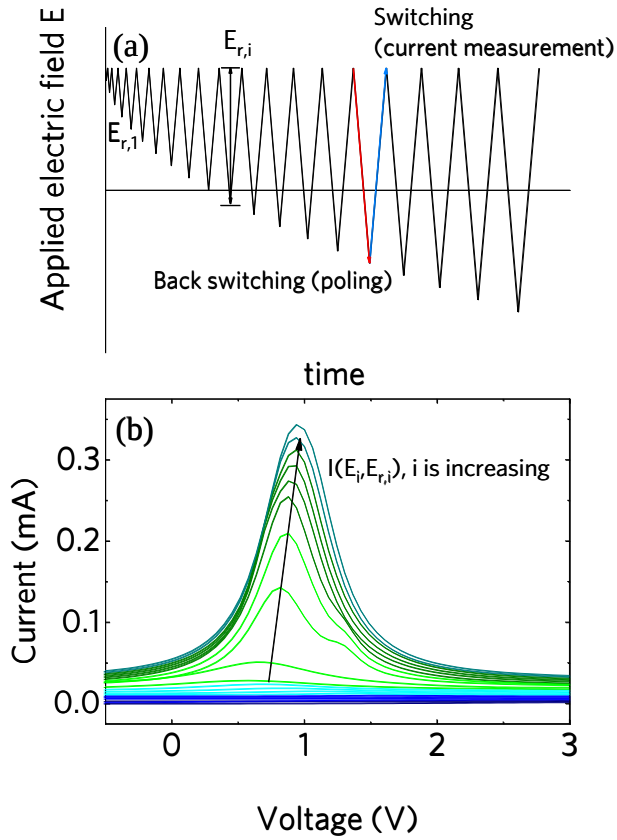

Fig. A1. (a) Schematic of electric field evolution along time for the first order reversal curve (FORC) measurement. Red arrow indicates the back switching field to pole the ferroelectric domain and blue arrow indicates the switching field for calculating switching density. (b) Corresponding transient current-voltage curves.

A.1.2. Detailed manual using keithley 4200 instrument

1. Make a new user test module to measure a capacitor structure using PMU modules and build the pulse train for back switching and switching by editing segment arb configuration (Fig. A2). It is recommended to make a same number of test module as i which represent sequence number of reversal field.

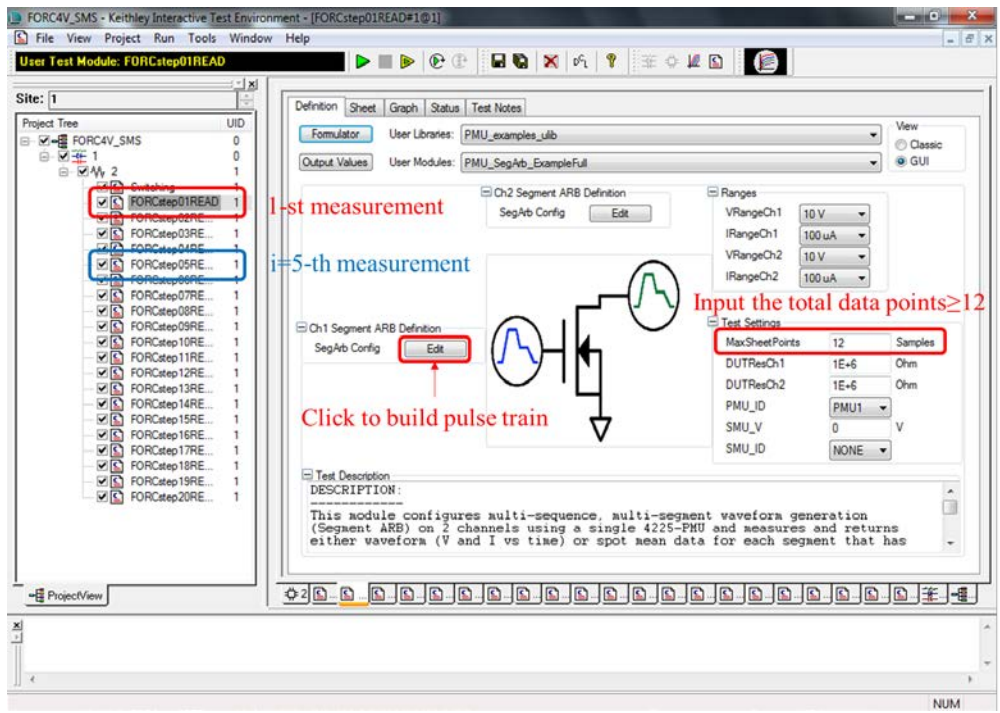

Fig. A2. User interface of keithley 4200. List of sequence of user test module for FORC measurement(Left) and parameter controller of 1-st measurement sequence.

2. The pulse train of i-th test module is made of a trapezoid pulse which starts at the saturated field and decreases to i-th reversal field and end at the saturated field again (Fig A3). The amplitude of reversal field should increase as arithmetic progression as increasing i until the reversal field equal to the opposite saturated field. The current data to calculate the switching density could be obtained by measuring the current during the switching process. The current data during the poling process is not necessary.

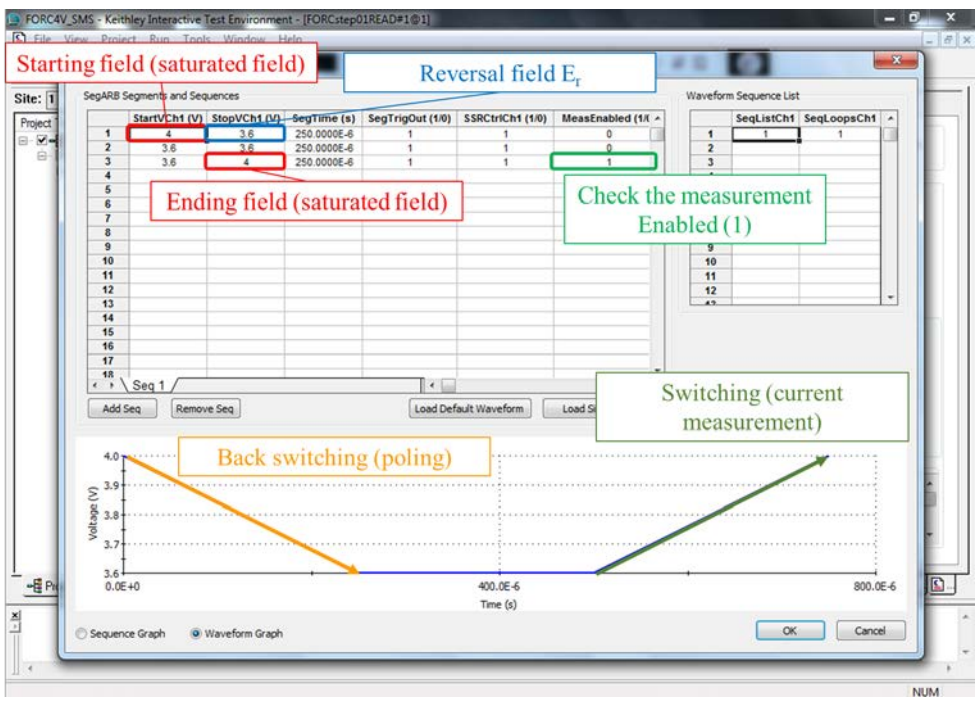

Fig. A3. Segment arb configuration of 1-st measurement sequence. The pulse train measurement can be manipulated by inputting amplitude, segment time, measurement enabled and etc.

3. Before applying pulse train, you have to adjust MaxSheetPoints in test setting. (Fig. A2.) Maxsheetpoints represent total points of data during the measurement and its minimum is 12. The current data should be obtained from each of the same actual field. Therefore, maxsheetpoints can be defined by multiplying of amplitude of reversal field by the maxsheetpoint of 1-st measurement, which represent how the FORC diagram shows distribution specifically. If you set the maxsheetpoints to $n \geq 12$ in 1-st measurement, the maxsheetpoints of i-th measurement should be $n \times i$.

4. Obtained current data should be aligned by actual field. It is recommended to calculate the FORC measurement with fitted data to minimize misaligning of the current data. The difference of the measured switching current response to the current for the previous reversal field can be calculated by subtracting the i-the data from (i-1)-the data (Fig. A4).

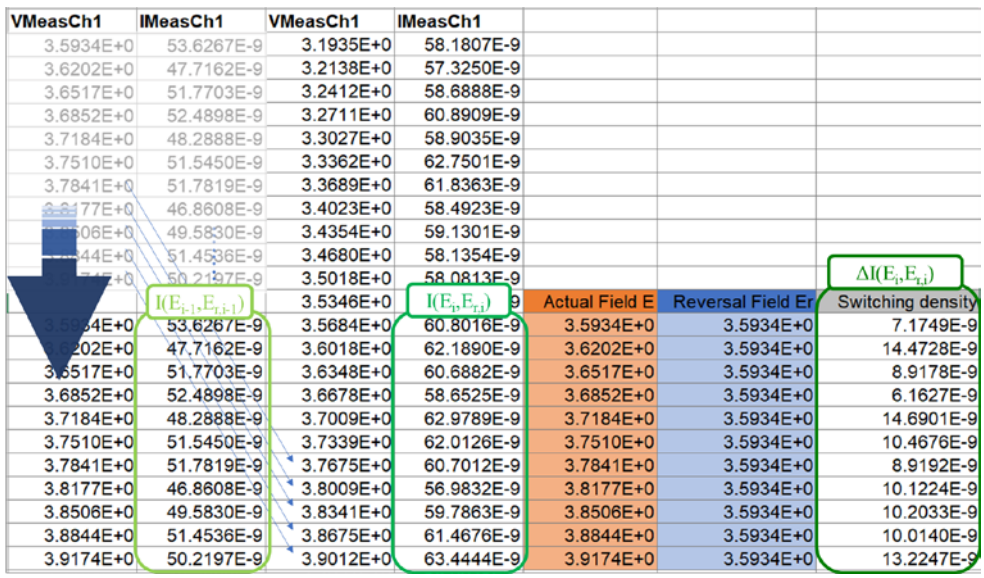

Fig. A4. Current-Voltage measurement data obtained by 1-st and 2-nd sequence of FORC measurement.

5. For each i-th reversal field $E_{r,i}$ plotted as the y-axis, plot the calculated switching density as the z-axis versus the actual field E as the x-axis.

6. You can represent the FORC distribution versus the coordinates of coercive voltage/field and the bias voltage/field by using coordinate transformation in eq. A2.

국문 초록

이 논문에서는 강유전성 스위칭 시간과 계면의 자유 전하 밀도와 관련하여 wake-up 현상과 split-up 현상에 대해 4.2% mol 실리콘 도핑 된 산화물 하프늄을 이용하여 연구하였다. Split-up에 앞서, 박막은 전기장 전계에 따라 잔류 분극이 증가하는 wake-up 현상을 보였다. Wake-up 현상 이후, 외부 전기장에 의해 잔류 분극 값이 감소하였고 강유전성 스위칭에 의한 전류 분포가 나누어지는 현상, 즉 split-up 현상을 보였다. Nucleation limited switching 모델을 기반으로 한 강유전성 스위칭 동역학을 통해 분석하였을때, 강유전성 핵생성을 위한 스위칭 시간은 wake-up과 split-up현상에 따라 각각 느려지고, 빨라졌다. 이와 함께 전압-전기용량 특성의 결과를 분석하였을 때, 박막내 결함의 증가가 split-up 현상에 영향을 주는 것으로 생각된다.

주요어 : 강유전체, 산화물 하프늄, Split-up, 박막, 결함
학번 : 2018-27202